



## Does CRA-40 outperform other reanalysis products in evaluating near-surface wind speed changes over China?

Cheng Shen<sup>a</sup>, Jinlin Zha<sup>b,c,\*</sup>, Jian Wu<sup>c</sup>, Deming Zhao<sup>b</sup>, Cesar Azorin-Molina<sup>d,e</sup>, Wenxuan Fan<sup>c</sup>, Yue Yu<sup>f</sup>

<sup>a</sup> Gaochun Meteorological Bureau, Nanjing 211300, People's Republic of China

<sup>b</sup> CAS Key Laboratory of Regional Climate and Environment for Temperate East Asia, Institute of Atmospheric Physics, Chinese Academy of Sciences, Beijing 100029, People's Republic of China

<sup>c</sup> Key Laboratory of Atmospheric Environment and Processes in the Boundary Layer over the Low-Latitude Plateau Region, Department of Atmospheric Science, Yunnan University, Kunming 650091, People's Republic of China

<sup>d</sup> Centro de Investigaciones sobre Desertificación, Consejo Superior de Investigaciones Científicas (CIDE-CSIC), Moncada, Valencia, Spain

<sup>e</sup> University of Gothenburg, Department of Earth Sciences - Regional Climate Group, Gothenburg, Sweden

<sup>f</sup> Nanjing Meteorological Bureau, Nanjing 210019, People's Republic of China

### ARTICLE INFO

#### Keywords:

Wind speed  
Reanalysis products  
CRA-40  
Terrestrial stilling  
Reversal

### ABSTRACT

Global reanalysis products have become essential tools employed towards the understanding of past climates, which are extensively employed by the wind energy industry to assess and develop wind resources. In this study, the terrestrial near-surface wind speed (NSWS) in the 40 year global reanalysis dataset released by China Meteorological Administration (CRA-40) was employed and compared with four state-of-the-art global reanalysis products, namely the European Centre for Medium-Range Weather Forecasts reanalysis version 5 (ERA5), National Centers for Environmental Prediction/National Center for Atmospheric Research reanalysis (NCEP1), National Centers for Environmental Prediction-Department of Energy reanalysis (NCEP2), and the Japanese 55 year reanalysis (JRA55). Large discrepancies were revealed among the reanalysis products in NSWSs across China. CRA-40 captures the climatology, seasonal, interannual, and monthly changes, as well as the terrestrial stilling compared with the recent observed increase. In contrast, NCEP1 and NCEP2 fail to reproduce the climatology and monthly changes in the observed NSWSs. Although JRA55 captures the terrestrial stilling in observations, it underestimates the mean value of NSWS. Therefore, CRA-40 provides the best agreement with stronger and more significant correlations against the observations when compared to other reanalysis products, and reproduces the observed multi-decadal variability. Thus, CRA-40 is the optimal choice to investigate NSWS with high spatial and temporal resolution across China, with a wide array of socioeconomic and environmental impacts.

### 1. Introduction

Terrestrial near-surface wind speed (NSWS) is a key component depicting changes in atmospheric circulation. Investigation of the variability of NSWSs provides theoretical insight into regional evapotranspiration, water cycle, visibility, dust storms, and air pollution (Liu et al., 2014; Wang et al., 2017; Zhang et al., 2020). Furthermore, the changes in NSWS directly determine the evaluation and development of wind energy (Tian et al., 2019; Pryor et al., 2020). Several studies have shown

that a decrease of 1–5% in NSWS can cause a loss of 1.7–8.6% in wind energy (He et al., 2010). Accompanied by the slowdown of NSWS over China, the mean wind energy declined by  $-3.84 \text{ W m}^{-2} \text{ decade}^{-1}$  due to changes in anthropogenic land use (Li et al., 2008).

A long-term reduction in NSWS has been reported at a global scale (Vautard et al., 2010; McVicar et al., 2012; Wu et al., 2018a; Zhang et al., 2019), and regional slowdowns in NSWSs are also commonly reported, including in Spain and Portugal (Azorin-Molina et al., 2014, 2016), Turkey (Dadaser-Celik and Cengiz, 2014), South Korea (Kim and

; NSWS, near-surface wind speed.

\* Corresponding author at: CAS Key Laboratory of Regional Climate and Environment for Temperate East Asia, Institute of Atmospheric Physics, Chinese Academy of Sciences, Beijing 100029, People's Republic of China.

E-mail address: zhajl@tea.ac.cn (J. Zha).

Paik, 2015; Chen et al., 2020), Finland (Laapas and Venalainen, 2018), Canada (Wan et al., 2010), America (Pryor et al., 2009; Pryor and Ledolter, 2010; Malloy et al., 2015), and Australia (McVicar et al., 2008). Roderick et al. (2007) used the term “stilling” to describe the reduction in NSWS. However, a weak increase in NSWS has also been observed in recent decades, and Zeng et al. (2019) used the term “reversal” to describe the increase in NSWS. In China, the terrestrial stilling or reversal is also extensively reported (Guo et al., 2011; Wu et al., 2016; Li et al., 2018; Zha et al., 2019a, 2021a; Zhang and Wang, 2020; Zhang et al., 2021).

Global reanalysis products are essential tools used to investigate past climate change in different disciplines (Ramon et al., 2019). Reanalysis products are the results of combining a frozen state-of-the-art numerical model with the assimilation of past observations from several sources to produce a consistent dataset over a long period of time (Fujiwara et al., 2017). With reanalysis products, variabilities or trends in variables can be inferred. One of the limitations of station-based wind speed series is that they only represent features of a site-specific location. Reanalysis datasets supply dynamically gridded wind data, which are particularly useful in areas with lack of observations. To determine whether terrestrial stilling and reversal at a global scale can be captured by reanalysis products, Fan et al. (2021) conducted an assessment of climatological winds and trends in five reanalysis products, namely the European Centre for Medium-Range Weather Forecasts (ECMWF) reanalysis version 5 (ERA5), the ECMWF reanalysis from January 1989 onward (which has been extended back to January 1979) (ERA-Interim), the Modern-Era Retrospective Analysis for Research and Applications version 2 (MERRA-2), the Japanese 55 year atmospheric reanalysis developed by the Japan Meteorological Agency (JRA55), and the Climate Forecast System version 2 (CFSv2). In that assessment, ERA5 most closely matched the observed climatological winds (Fan et al., 2021). However, all reanalysis products fail to effectively capture the stilling or recent reversal of stilling (Deng et al., 2021; Fan et al., 2021). A comparison of reanalysis products that simulate the climatology and trends in NSWSs over China showed that the trends in NSWS are best captured with JRA55 (Wang et al., 2020; Zhang and Wang, 2020). Nevertheless, large discrepancies were found among reanalysis datasets when the climatology and long-term trends in NSWS were compared between observations and reanalysis products. According to our knowledge, no reanalysis product succeeds to efficiently reproduce the spatiotemporal changes of the observed NSWS over China.

Reanalysis products have inherent uncertainties derived from model simplifications, observational uncertainties, and the data assimilation procedure (Ramon et al., 2019). A comprehensive verification of NSWS features in different reanalysis products is strongly required to facilitate simulations of the regional climate and investigations of ecological and environmental issues associated with NSWS. Furthermore, reanalysis datasets are also useful in evaluating and developing wind energy, particularly in regions where the observations are lacking (Sherman et al., 2021). Previous studies primarily focused on the capabilities of reanalysis products in simulating climatology and long-term trends in NSWS over China (Chen et al., 2012; Wang et al., 2020; Zhang and Wang, 2020), and an overall evaluation of the performance of main reanalysis products in simulating NSWS changes at different time scales yet to be conducted. Consequently, detailed analyses are required to determine which global reanalysis products better capture the variations in NSWS over China.

The National Meteorological Information Center (NMIC) of the China Meteorological Administration (CMA) recently developed a 40 year global reanalysis (CRA-40) dataset (Liang et al., 2020). The CRA-40 dataset represents China’s first generation of a global atmospheric reanalysis product. Whether the CRA-40 is sufficient to quantify regional changes in NSWS remains unknown. The assessment of CRA-40 is essential, as almost all reanalysis products fail to reproduce the variations in NSWS over China (Zhang and Wang, 2020). This study sets out to answer one key issue: what are the quantitative differences between

CRA-40 and other most widely used reanalysis products in estimating the climatology, interannual variabilities, seasonal and decadal changes in NSWS over China? The results provide guidance in selecting a reanalysis dataset to estimate wind resources and ecological and environmental issues associated with NSWS.

## 2. Datasets and methods

### 2.1. Datasets

To evaluate the performance of reanalysis products in simulating the NSWS changes over China, the gridded monthly-scale CN05.1 observational database is used. The spatial resolution of CN05.1 is  $0.25^\circ \times 0.25^\circ$ . CN05.1 is widely used for the analysis of observed climate characteristics over China and assessment of global and regional model performance. Hence, it has been validated as a reliable method (Wu et al., 2012; Sun and Wang, 2014; Bucchignani et al., 2016). Details on the CN05.1 dataset are provided by Wu and Gao (2013). To validate the performance of the CN05.1 dataset, another observation dataset is also selected (<http://www.nmic.cn/data/cdcindex/cid/6d1b5efbdcbf9a58.html>; last accessed 30th October 2021). The dataset was examined and calibrated by the NMIC of the CMA. To obtain a high-quality wind speed record at each station, strict quality control and a homogenization test for wind speed were performed in the previous study (Shen et al., 2021a). To facilitate description, the homogenized dataset is named Obs\_Hom. Details of wind speed quality control and homogenization test for Obs\_Hom are presented in Shen et al. (2021a). The daily mean wind speed record in Obs\_Hom can be obtained only from 1970 to 2010, such that the reversal of terrestrial stilling could not be observed. Consequently, the Obs\_Hom dataset was only used to compare and evaluate the quality of the CN05.1 database.

CRA-40 covers the period from 1979 to 2020 (Zhao et al., 2021), which uses the National Centers for Environmental Prediction (NCEP) Global Forecast System/Grid-point Statistical Interpolation 3D-Var system with 64 vertical levels and horizontal resolution of 34 km (Li et al., 2020; Liang et al., 2020). CRA-40 was compared with four major reanalysis products, specifically 1) the ECMWF reanalysis version 5 (ERA5; Hersbach et al., 2020), 2) the National Centers for Environmental Prediction/National Center for Atmospheric Research reanalysis (NCEP1; Kalnay et al., 1996), 3) the National Centers for Environmental Prediction-Department of Energy reanalysis (NCEP2; Kanamitsu et al., 2002), and 4) the Japanese 55 year atmospheric reanalysis developed by the Japan Meteorological Agency (JRA55; Kobayashi et al., 2015). The daily mean values of all datasets were used. Details for the reanalysis products are presented in Table 1.

### 2.2. Methods

To evaluate whether the reanalysis products can reproduce the observed terrestrial stilling versus recent reversal of stilling, a piecewise linear function (PWLF) was used to fit the trends of NSWS during different periods. The PWLF can automatically detect the point at which the slope of a linear function changes and identify optimal breakpoints, allowing multiple linear models to be fitted to each distinct section of a time sequence (Fyllas et al., 2009; Jekel and Venter, 2019; Shen et al., 2021b). A PWLF can be described using Eq. (1).

$$y(t) = \begin{cases} \eta_1 + m_1(t - b_1) & b_1 < t < b_2 \\ \eta_2 + m_2(t - b_2) & b_2 < t < b_3 \\ \eta_{\eta_b-1} + m_{\eta_b-1}(t - b_{\eta_b-1}) & b_{\eta_b-1} < t < b_{\eta_b} \end{cases} \quad (1)$$

where  $b_1$  is the location of the first breakpoint,  $b_2$  is the location of the second breakpoint, and until the last breakpoint  $b_{\eta_b}$ . In cases where the breakpoint locations are unknown, optimization is used to identify the best set of breakpoint locations that minimizes the overall sum-of-square of the residuals (SSR). The SSR can be represented as a function

**Table 1**

Main characteristics of five reanalysis products.

	CRA-40	ERA5	NCEP1	NCEP2	JRA55
Production centre	China Meteorological Administration (CMA)	European Centre for Medium-Range Weather Forecasts (ECMWF)	National Centers for Environmental Prediction (NCEP) and National Center for Atmospheric Research (NCAR)	National Centers for Environmental Prediction (NCEP)-Department of Energy (DOE)	Japan Meteorological Agency (JMA)
Spatial resolution	$1.0^\circ \times 1.0^\circ$	$0.25^\circ \times 0.25^\circ$	$2.5^\circ \times 2.5^\circ$	$2.5^\circ \times 2.5^\circ$	$1.25^\circ \times 1.25^\circ$
Temporal resolution	3-hourly	1-hourly	6-hourly	6-hourly	3-hourly
Temporal coverage	1979-present	1950-present	1948 to present	1979-present	1958-present
Analysis scheme	3D-Var	4D-Var	3D-Var	3D-Var	4D-Var
URL	<a href="http://data.cma.cn/analysis/cra40">http://data.cma.cn/analysis/cra40</a>	<a href="https://www.ecmwf.int/">https://www.ecmwf.int/</a>	<a href="http://www.esrl.noaa.gov/">http://www.esrl.noaa.gov/</a>	<a href="http://www.esrl.noaa.gov/">http://www.esrl.noaa.gov/</a>	<a href="http://jra.kishou.go.jp/">http://jra.kishou.go.jp/</a>

dependent on the breakpoint locations. The optimization problem is summarized in Eq. (2):

$$\begin{cases} \text{minimize } SSR(\mathbf{b}), \mathbf{b} = [b_2, \dots, b_{nb-1}]^T \\ \text{subject to } x_1 \leq b_k \leq x_n, k = 1, 2, \dots, b_n. \end{cases} \quad (2)$$

In the PWLF, differential evolution is used for global optimization (Storn and Price, 1997). Details for the PWLF are provided by Jekel and Venter (2019).

To evaluate the performance of reanalysis products in simulating the NSWS changes, the correlation coefficient, wind speed difference (WSD), skill score, and root mean square error (RMSE) between observations and reanalysis products are analyzed. The correlation coefficient, WSD, and RMSE have been used in a previous study (Shen et al., 2021a), hence, we herein we omit the details. The skill score is used to quantify the performance of reanalysis products in simulating NSWS changes and is calculated using Eq. (3).

$$\text{Skill score} = \frac{(1 + R)^2}{\left( SDR + \frac{1}{SDR} \right)^2} \quad (3)$$

where  $R$  is the spatial correlation coefficient between the observation and reanalysis product, and  $SDR$  is the ratio of the spatial standard deviations of the observation and reanalysis product. Both the spatial distribution and magnitude are considered in Eq. (3). Theoretically, the skill score is located between zero and one. For better the relations, the value approaches one (Song and Zhou, 2014; Peng et al., 2020). To facilitate the intercomparison of spatiotemporal characteristics among datasets, all datasets are interpolated to  $2.5^\circ \times 2.5^\circ$  spatial resolution based on the bilinear interpolation method. The linear trend is calculated using the least square method, and the two-tailed Student's  $t$ -test was used to determine the significance of the results (Zha et al., 2016). The interannual fluctuation of NSWS was defined as the year-to-year NSWS difference. To quantify the consistency of interannual changes, the probability of extremes appearing at the same time point (PEST) between the observation and reanalysis product was calculated (Zha et al., 2019b). The spatial mean value of NSWS was equal to the total wind speed divided by total grids over China. The four boreal seasons are winter (December, January, and February), spring (March, April, and May), summer (June, July, and August), and autumn (September,

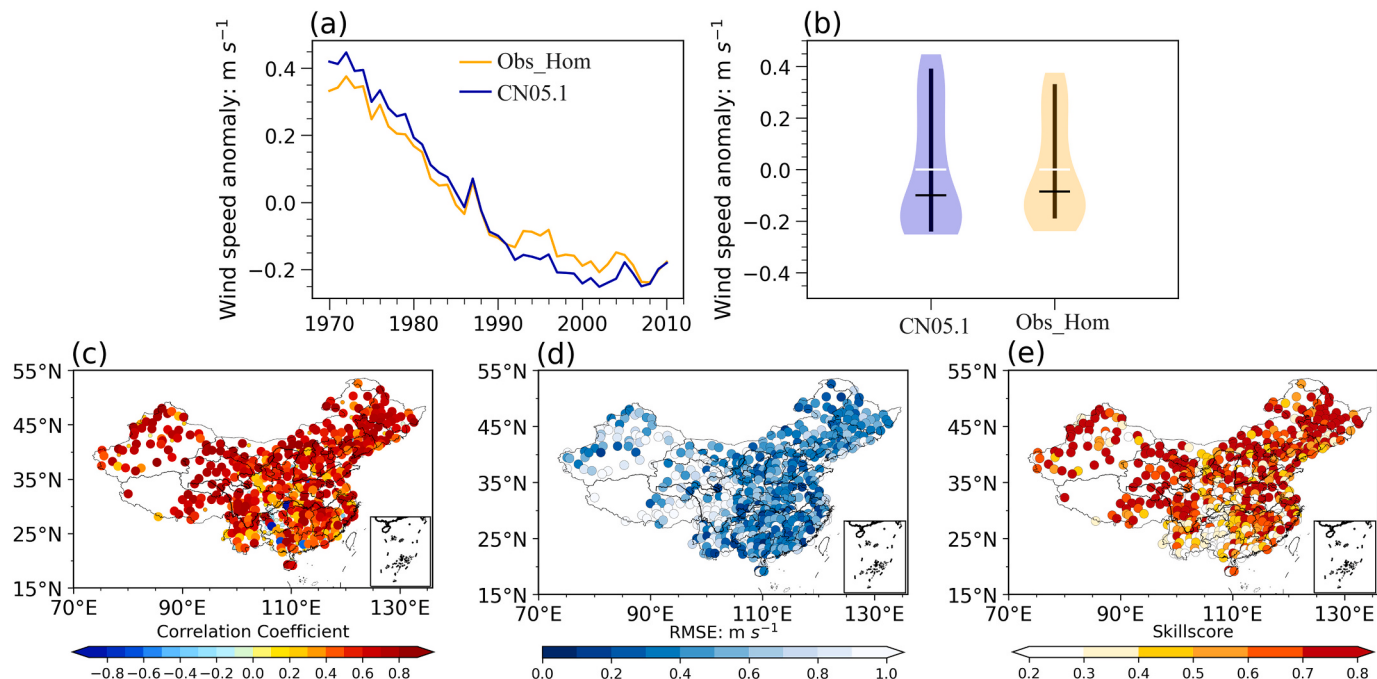


**Fig. 1.** (a) Temporal changes in NSWS anomalies (unit:  $\text{m s}^{-1}$ ) in two observational datasets and (b) violin plot of NSWS anomalies, (c) correlation coefficients, (d) root mean square errors, and (e) skill scores between the two observational datasets. In (b), white lines denote mean values; black lines denote median values; and whiskers show the 10th and 90th percentiles of NSWS. Shading represents the full distribution of the data. Wider sections of the violin plot represent a higher probability of NSWSs at that given value, whereas thinner sections correspond to a lower probability.

October, and November).

### 3. Results

#### 3.1. Comparisons of different observational datasets

Although CN05.1 has been validated as a credible observational dataset (Wu et al., 2012; Wu and Gao, 2013), the performance of the dataset was further evaluated by comparison with another dataset (Fig. 1). The two observational datasets showed the same interannual and decadal changes from 1970 to 2010, with a correlation coefficient of 0.99 ( $P < 0.001$ ; Fig. 1a). The CN05.1 violin plot was consistent with that of the homogeneous NSWSs (Fig. 1b). The median values of NSWSs were below the mean values, and the probability distributions of the two observational datasets were also consistent. CN05.1 and homogeneous NSWS datasets were mainly positively correlated over China, with most correlation coefficients were significant at the 0.10 level, according to the *t*-test (Fig. 1c). In most regions, the correlation coefficients were above 0.60 ( $P < 0.001$ ), and the RMSE was below  $0.60 \text{ m s}^{-1}$ . The largest RMSE values were located mainly in the Tibetan Plateau, reaching  $0.8 \text{ m s}^{-1}$ , whereas the smallest values ( $< 0.6 \text{ m s}^{-1}$ ) were located mainly in eastern China (Fig. 1d). The skill score between the two observational datasets was larger than 0.6 in most parts of China (Fig. 1e). Based on these results, the NSWSs in the two observational datasets showed consistent spatiotemporal changes. Hence, the quality of the wind speed data in the CN05.1 dataset is high.

#### 3.2. Climatology of NSWSs from observation and reanalysis

Spatial patterns of the NSWS in observation and reanalysis products are shown in Fig. 2. The spatial distributions of mean values in CRA-40 (Fig. 2b) and ERA5 (Fig. 2c) were similar to those of the observations (Fig. 2a). The strongest NSWS occurred mainly in Inner Mongolia, northeastern China, and Tibetan Plateau region, whereas the weakest values occurred mainly in central, southwestern, and southeastern China. NCEP1, NCEP2, and JRA55 captured the spatial patterns of the

observed NSWSs. However, the NSWSs in NCEP1 and NCEP2 were smaller than those observed over Inner Mongolia and the middle and lower reaches of the Yellow River (Fig. 2d and e). The NSWS in JRA55 was smaller than that observed across China (Fig. 2f). The spatial correlation coefficients between observations and reanalysis products were 0.68 ( $P < 0.01$ ) for CRA-40, 0.55 ( $P < 0.01$ ) for ERA5, 0.22 ( $P < 0.01$ ) for NCEP1, 0.30 ( $P < 0.01$ ) for NCEP2, and 0.53 ( $P < 0.01$ ) for JRA55. Thus, compared to other reanalysis products, the spatial distribution of mean NSWS was better reproduced by CRA-40. The mean values and variances of seasonal NSWSs in the observations and reanalysis products were also compared (Table 2). The mean values of seasonal NSWSs in CRA-40 and ERA5 were closer to the observation than the other reanalysis products. However, compared to CRA-40, the mean value and variance of NSWS in ERA5 were closer to observations. Notably, the CRA-40 and ERA5 underestimated the interannual variabilities in NSWSs during all four seasons. Details are shown in Table 2.

We compared the spatial distributions of NSWS trends in the observations and five reanalysis products (Fig. 3). A slowdown in NSWS was observed from 1979 to 2017 (Fig. 3a). The strongest decreases occurred mainly in northern and eastern China, in which the decreasing trend reached  $-0.20 \text{ m s}^{-1} \text{ decade}^{-1}$  ( $P < 0.10$ ). CRA-40 also showed a reduction in the NSWS, especially in northern, northeastern, and eastern China. However, CRA-40 exhibited an increase in NSWS in some regions of western China, which failed to reproduce the observed reduction in NSWS in those regions (Fig. 3b). ERA5 failed to reproduce the decrease in NSWS across all of China (Fig. 3c). The NSWS trend in NCEP1 was likewise not consistent with that in NCEP2. For example, NSWSs trends in NCEP1 clearly differed from those of NCEP2 over southwestern China and western Inner Mongolia. Furthermore, the NSWSs in NCEP1 and NCEP2 showed upward trends in the northwestern China and the vicinity of Huaihe River basin, and these features were not consistent with the observations in those regions (Fig. 3d and e). JRA55 captured the terrestrial stilling over eastern China and the Tibetan Plateau, but showed increasing trends in NSWS over the middle reaches of the Yellow River and northwestern China (Fig. 3f). Overall, the spatial pattern of the observed NSWS trends was better reproduced by CRA-40 and JRA55

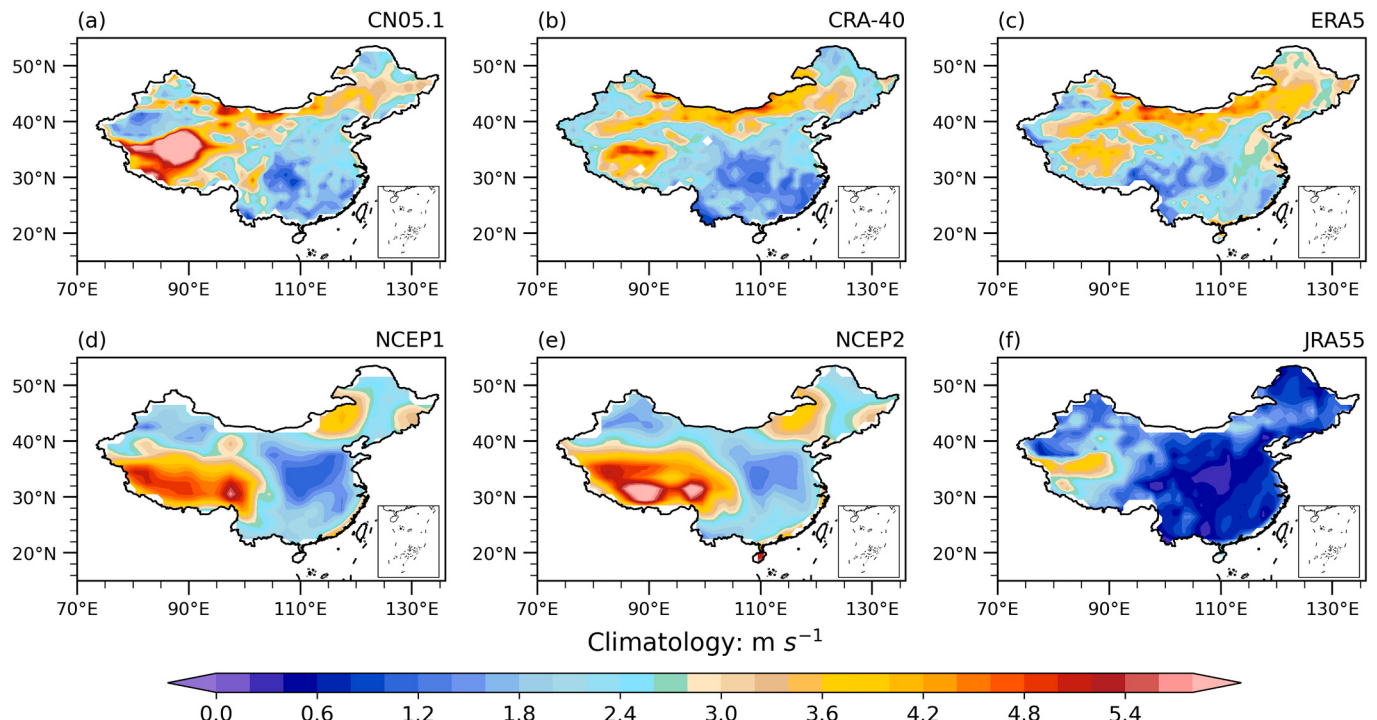


**Fig. 2.** Spatial patterns of annual mean NSWS (unit:  $\text{m s}^{-1}$ ) from 1979 to 2017 in (a) observational database CN05.1 and reanalysis products (b) CRA-40, (c) ERA5, (d) NCEP1, (e) NCEP2, and (f) JRA55.

**Table 2**

Mean, variance, and 10th, 50th, and 90th percentiles of seasonal mean NSWSs (unit:  $\text{m s}^{-1}$ ) in observations and five reanalysis products.

		Mean value	Variance	50th percentile of NSWS	10th percentile of NSWS	90th percentile of NSWS
Winter	Observation	2.75	0.0381	2.70	2.57	2.98
	CRA-40	2.32	0.008	2.33	2.21	2.42
	ERA5	2.69	0.007	2.67	2.60	2.81
	NCEP1	3.55	0.026	3.53	3.35	3.80
	NCEP2	3.69	0.035	3.68	3.47	3.96
	JRA55	1.75	0.001	1.77	1.72	1.78
Spring	Observation	3.36	0.046	3.27	3.13	3.67
	CRA-40	2.87	0.011	2.88	2.73	2.97
	ERA5	3.05	0.005	3.06	2.95	3.12
	NCEP1	2.54	0.027	2.54	2.31	2.76
	NCEP2	2.69	0.040	2.71	2.42	2.95
	JRA55	1.53	0.001	1.56	1.49	1.56
Summer	Observation	2.79	0.026	2.73	2.63	3.05
	CRA-40	2.45	0.007	2.44	2.34	2.58
	ERA5	2.61	0.002	2.61	2.57	2.69
	NCEP1	2.23	0.024	2.23	2.02	2.46
	NCEP2	2.58	0.028	2.56	2.37	2.83
	JRA55	1.12	0.007	1.17	1.03	1.18
Autumn	Observation	2.63	0.024	2.58	2.47	2.84
	CRA-40	2.33	0.007	2.32	2.24	2.44
	ERA5	2.61	0.003	2.60	2.56	2.68
	NCEP1	2.56	0.018	2.56	2.40	2.72
	NCEP2	2.66	0.013	2.66	2.53	2.78
	JRA55	1.37	0.001	1.38	1.33	1.41

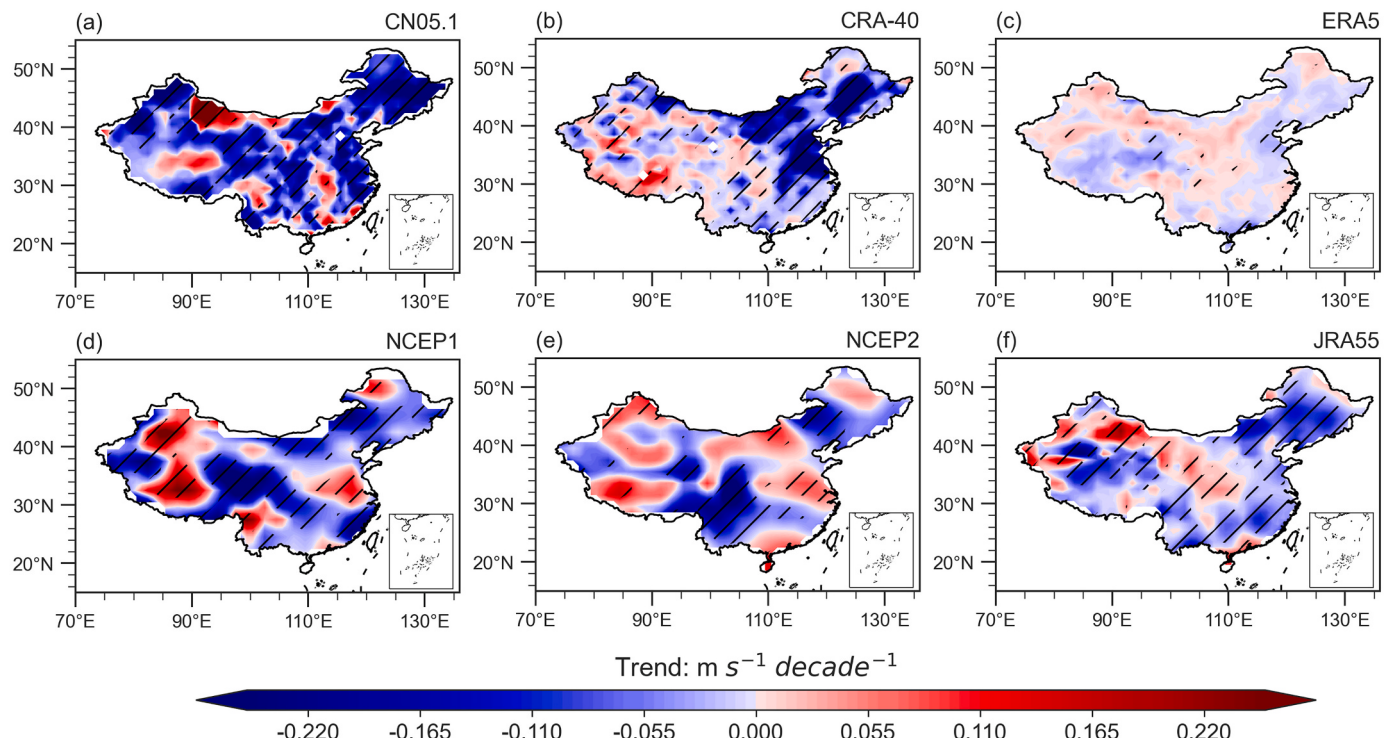


**Fig. 3.** Spatial patterns of the trend in annual mean NSWS (unit:  $\text{m s}^{-1} \text{decade}^{-1}$ ) from 1979 to 2017 in (a) observational database CN05.1 and reanalysis products (b) CRA-40, (c) ERA5, (d) NCEP1, (e) NCEP2, and (f) JRA55. Diagonal lines denote significant trends significant at the 0.10 level, according to t-test.

than other reanalysis products. However, the performance of both CRA-40 and JRA55 was weaker in simulating terrestrial stilling over western China than over eastern China. This discrepancy can be attributed to inadequate simulation of heterogeneous terrain and atmospheric boundary layer conditions over western China in the process of data assimilation (Fan et al., 2021), and the low number of observations assimilated by the CRA-40 and JRA55.

The probability density function (PDF) of spatial mean NSWS in the observations and different reanalysis products was evaluated (Fig. 4a). The PDF of NSWS in JRA55 clearly shifted leftward. The NSWSs

corresponding to the maximums of the PDFs in observations, CRA-40, ERA5, NCEP1, NCEP2, and JRA55 were  $2.12, 2.17, 2.76, 2.14, 2.15$ , and  $0.75 \text{ m s}^{-1}$ , respectively. When the 50th percentile of the observed NSWSs ( $2.64 \text{ m s}^{-1}$ ) was considered as the baseline, the probabilities of NSWSs exceeding  $2.64 \text{ m s}^{-1}$  in CRA-40, ERA5, NCEP1, NCEP2, and JRA55 were  $47.14, 53.94, 44.13, 48.36$ , and  $15.86\%$ , respectively. Therefore, compared with that in JRA55, the PDFs of NSWSs in CRA-40, ERA5, NCEP1, and NCEP2 were closer to observations. However, it is also noted that the CRA-40, ERA5, and JRA55 cannot well capture the observed strong winds, i.e., above  $5 \text{ m s}^{-1}$ , whereas other reanalysis

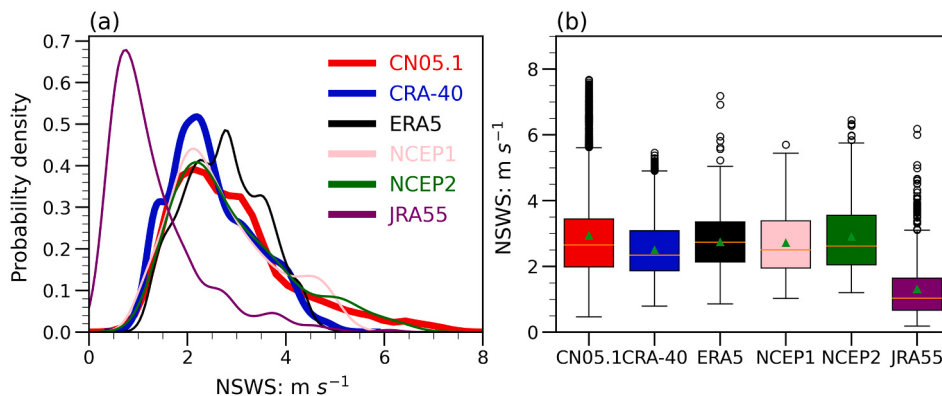


**Fig. 4.** (a) Probability density function of spatial mean values in NSWSSs, and (b) box-and-whisker plots of spatial mean values in NSWSSs. The mean (central triangle), median (middle lines), 10th and 90th percentile ranges (boxes), maximum and minimum values (upper and lower horizontal lines), and the outliers (circles) are presented in the box-and-whisker plot.

products do, e.g., NCEP1 and NCEP2 (Fig. 4a). Box-and-whisker plots were employed to evaluate the performance of reanalysis products in simulating the NSWSSs change during the study period (Fig. 4b). The strongest wind episodes were exhibited in the observations, followed by those in NCEP2 and CRA-40, and the weakest wind episodes were presented in JRA55. The mean values of NSWSSs were larger than the median values, and this feature was characteristic of the observations and all reanalysis products, but for ERA5. Therefore, in the comparisons with the PDFs and box-and-whisker plots, the performance of JRA55 in simulating the changes in NSWSSs was weaker than that of the other reanalysis products. Details on the medians, 10th, and 90th percentiles of seasonal mean NSWSSs in the observations and reanalysis products are presented in Table 2.

### 3.3. Temporal changes in NSWSSs from observation and reanalysis

Temporal evolutions in annual and seasonal mean NSWSSs in the observations and reanalysis products are shown in Fig. 5. There was a significant decrease in the observed NSWSS from 1979 to 2017, with decreasing trends of  $-0.104$  ( $P < 0.01$ ),  $-0.063$  ( $P < 0.01$ ),  $-0.155$  ( $P < 0.01$ ),  $-0.098$  ( $P < 0.01$ ), and  $-0.091$  ( $P < 0.01$ )  $\text{m s}^{-1}$  decade $^{-1}$  in the annual mean, winter, spring, summer, and autumn, respectively. As for CRA-40, the changes in annual and seasonal mean NSWSSs were partially consistent with those of the observations. Compared with other reanalysis products, the temporal evolutions of NSWSSs in CRA-40 were closer to those of the observations, although the NSWSSs in CRA-40 were lower than those in the observations. The NSWSSs in CRA-40 showed decreases of  $-0.051$  ( $P < 0.01$ ),  $-0.019$  ( $P < 0.10$ ),  $-0.064$  ( $P < 0.01$ ),  $-0.065$  ( $P < 0.01$ ), and  $-0.051$  ( $P < 0.01$ )  $\text{m s}^{-1}$  decade $^{-1}$  for the annual mean, winter, spring, summer, and autumn, respectively. The reductions in NSWSSs were not found in ERA5. The NSWSSs in NCEP1 and NCEP2 exhibited seasonal differences. For the annual mean and autumn (Fig. 5a and e), the NSWSSs in NCEP1 and NCEP2 were close to those of the observations and also showed decreasing trends. However, the NSWSS in NCEP2 was larger than that of the observations during winter (Fig. 5b) and smaller during spring (Fig. 5c). In JRA55, the long-term trends in NSWSSs were decreasing in all seasons, with trends of  $-0.023$  ( $P < 0.01$ ),  $-0.0067$  ( $P > 0.10$ ),  $-0.043$  ( $P < 0.01$ ),  $-0.023$  ( $P < 0.01$ ), and  $-0.020$  ( $P < 0.05$ )  $\text{m s}^{-1}$  decade $^{-1}$  for the annual mean, winter, spring, summer, and autumn, respectively. However, the NSWSS in JRA55 were lower than the observations in four seasons. Furthermore, the interannual fluctuations of NSWSSs in CRA-40 were closer to observation than that in NCEP1 and NCEP2. NCEP1 and NCEP2 overestimated the interannual fluctuations in the observed NSWSSs. The PESTs between CRA-40 and the observation reached 56.10, 52.63, 44.74, 50.00, and 47.37% in the annual mean, winter, spring, summer, and autumn, respectively, and these values were larger than those between the observation and the

other reanalysis products (Fig. 6).

The ability of reanalysis datasets to simulate changes in the monthly wind speed is likewise crucial because of the different implications of such changes. The observed NSWSS strengthened from January to April and then weakened from April to December, and CRA-40 and ERA5 produced similar changes in the monthly NSWSSs. However, monthly mean NSWSSs in NCEP1, NCEP2, and JRA55 were not consistent with those of the observations and primarily decreased from January to August and increased from August to December (Fig. 7a). In a comparison of the trends of monthly NSWSSs between the observations and reanalysis products (Fig. 7b), CRA-40 effectively captures the decreasing trends. ERA5 and JRA55 fail to reproduce the significant decrease in monthly NSWSSs. Although NCEP1 and NCEP2 reproduce the downward trends in monthly NSWSSs (Fig. 7b), the monthly changes in NSWSSs by NCEP1 and NCEP2 were not consistent with those of the observations (Fig. 7a). Therefore, the seasonal, interannual, and monthly changes in the observed NSWSSs over China were best reproduced by CRA-40.

### 3.4. Quantitative relations between observations and reanalysis products

To quantitatively evaluate the relations between the observations and reanalysis products, the correlation coefficient, WSD, RMSE, and skill score between observations and reanalysis datasets were analyzed (Fig. 8). All reanalysis products and observations showed positive correlations. Annually and seasonally, the most significant correlation coefficients were found in JRA55. The correlation coefficients of annual and seasonal mean NSWSSs between the observations and CRA-40 were significant at the 0.10 level, according to the *t*-test. However, the correlation coefficients between CRA-40 and the observations by month were more higher than those for the annual and seasonal mean NSWSSs. Furthermore, the monthly correlation coefficients in CRA-40 were the most significant of all reanalysis products (Fig. 8a).

The WSDs between observations and CRA-40 and between the observations and JRA55 were negative (Fig. 8b), with the largest negative WSDs in JRA55. The WSDs in CRA-40 and ERA5 were smaller than that in other reanalysis products, and that the lowest WSDs were presented in ERA5. The WSDs in NCEP1 and NCEP2 were not consistently positive or negative, implying that NCEP1 and NCEP2 simulations of the climatology of NSWSSs were not labile at different time scales. Similar to WSDs, the RMSEs of CRA-40 and ERA5 were small and that of JRA55 was large (Fig. 8c). In a comparison of the correlation coefficient with RMSEs in JRA55, the simulation of the annual and seasonal mean NSWSSs was better than that of monthly mean NSWSS. CRA-40 had a larger skill score than other reanalysis products, especially for the monthly time scale, which reached the high skill score of 60.0% (Fig. 8d). On the basis of these results, CRA-40 exhibited the smallest differences in the same estimation indices at different time scales,

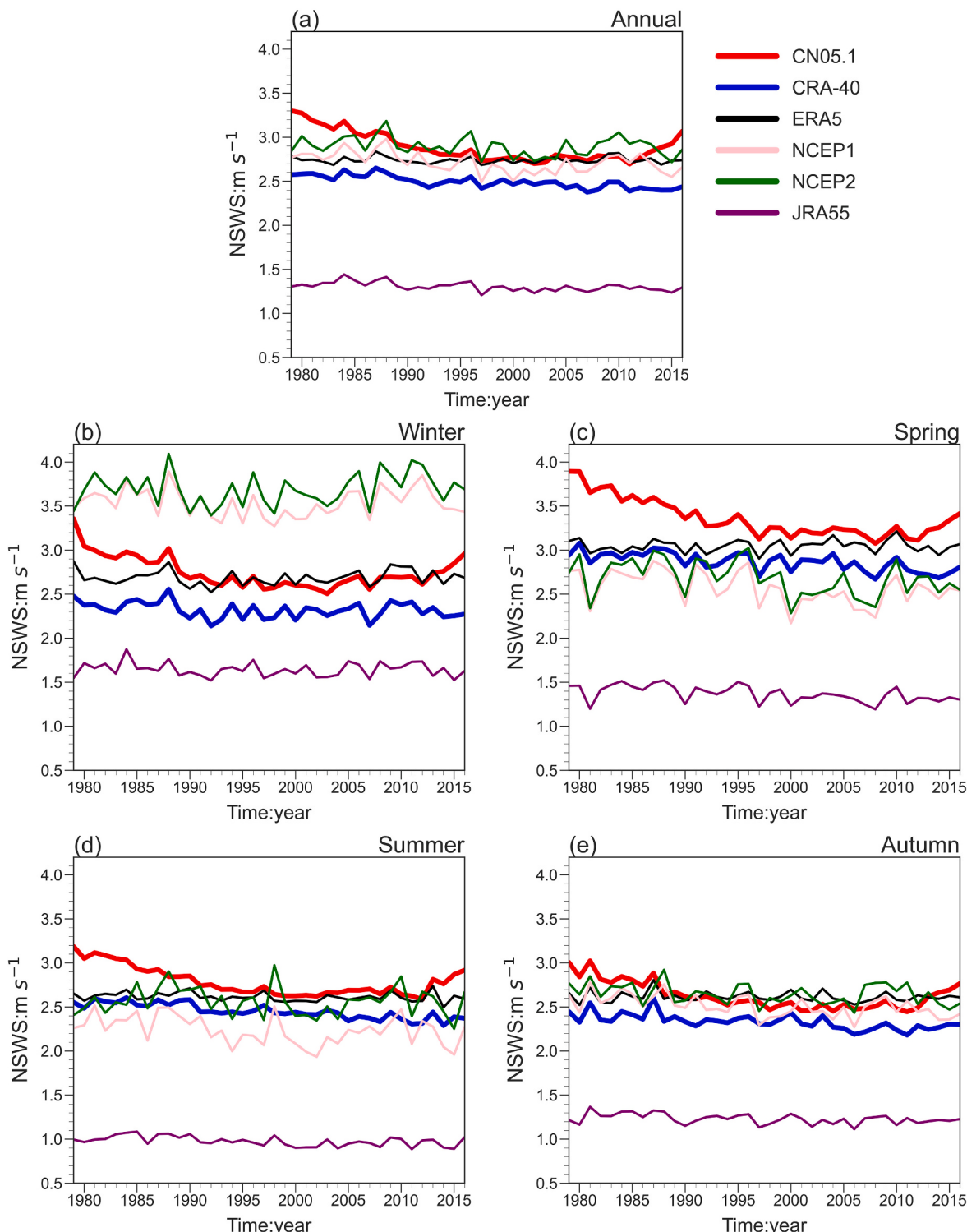


**Fig. 5.** Temporal evolutions in annual and seasonal mean NSWSs (unit:  $\text{m s}^{-1}$ ) in the observational database and different global reanalysis products. (a) annual mean, (b) winter, (c) spring, (d) summer, and (e) autumn.

compared with those in the other reanalysis products. Therefore, the changes in the observed NSWSs at different time scales were best simulated by CRA-40.

### 3.5. Terrestrial stilling versus recent reversal in CRA-40

Among the reanalysis products, CRA-40 provided the best representation of the variations in NSWS over China, including the

climatology, long-term trends, seasonal, interannual, and monthly changes in NSWS. A long-term slowdown in NSWS over China was reported (Xu et al., 2006; Jiang et al., 2010; You et al., 2010, 2014; Wu et al., 2017, 2018b,c; Zha et al., 2017a, 2017b); however, the observed NSWS increased in the recent decade (Li et al., 2018; Zhang and Wang, 2020; Ge et al., 2021; Zha et al., 2021a,a, Zha et al., 2021b). Therefore, whether CRA-40 could capture the terrestrial stilling versus recent reversal of stilling was evaluated. The PWLF indicating the temporal

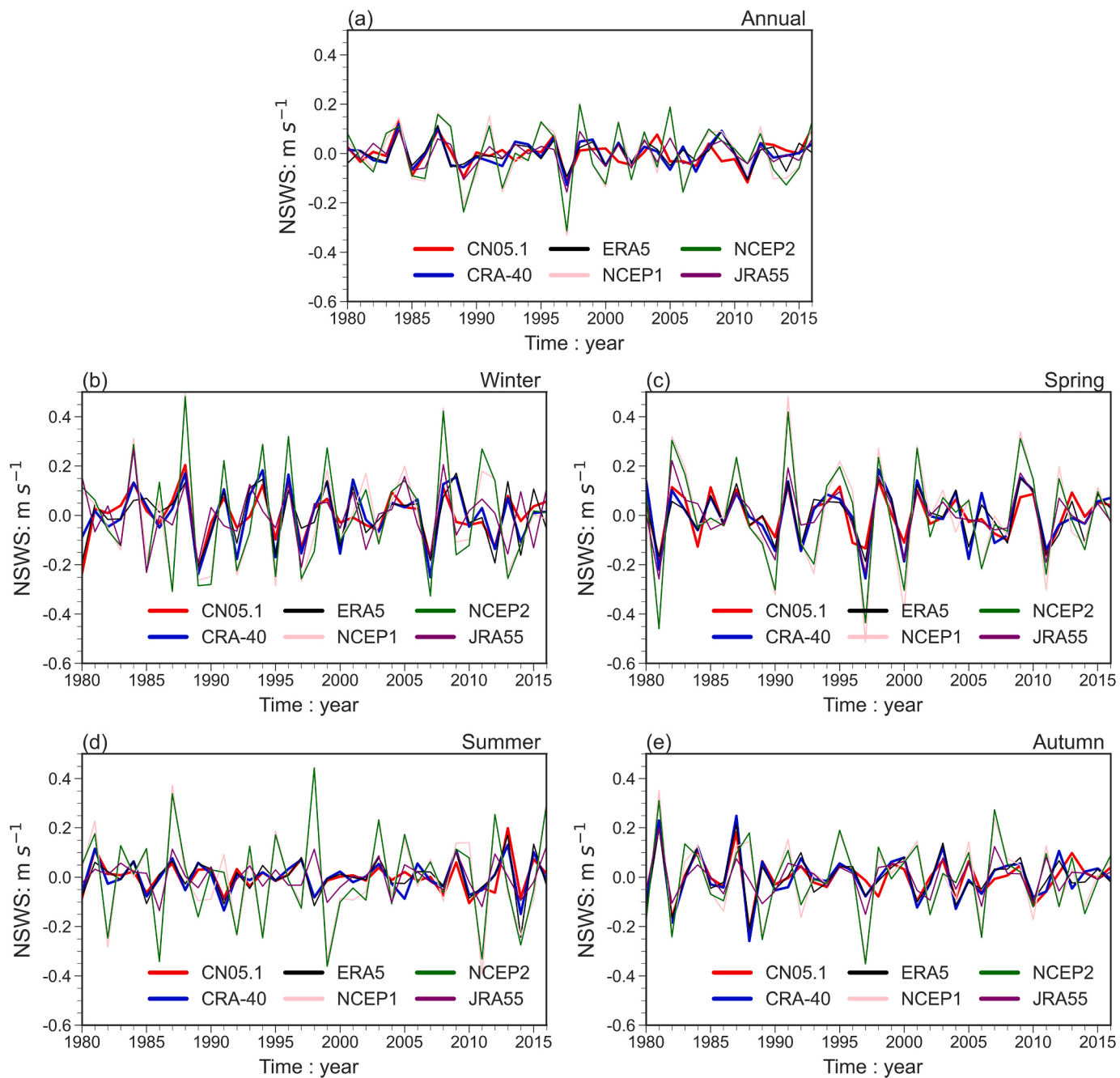


**Fig. 6.** Temporal evolutions of interannual fluctuation in NSWS (unit:  $\text{m s}^{-1}$ ) in the observational database and five reanalysis products. (a) annual mean, (b) winter, (c) spring, (d) summer, and (e) autumn. The interannual fluctuation of NSWS is defined as the year-to-year NSWS difference.

evolution in the observed NSWS during the entire study period was separated into two periods. The annual mean NSWS decreased in the period spanning 1979–2011 ( $-0.16 \text{ m s}^{-1} \text{ decade}^{-1}$ ;  $P < 0.001$ ) and increased from 2011 to 2016 ( $+0.86 \text{ m s}^{-1} \text{ decade}^{-1}$ ;  $P < 0.001$ ) (Fig. 9a). CRA-40 captured the terrestrial stilling versus reversal, although the increases in NSWSs after the turning points were weaker than those in the observations (Fig. 9b). In CRA-40, the annual mean NSWS decreased from 1979 to 2011 ( $-0.056 \text{ m s}^{-1} \text{ decade}^{-1}$ ;  $P < 0.001$ ) and increased from 2011 to 2016 ( $+0.031 \text{ m s}^{-1} \text{ decade}^{-1}$ ;  $P < 0.01$ ). To exclude the possibility that the turning points were caused by extremely large winds at only a few grids, the analyses were repeated 3000 times by randomly resampling 30% of all grids each time to validate the turning points (light blue lines in Fig. 9a and b). The turning points in each sample were close to those in the total sample. To further

demonstrate that CRA-40 can reproduce the stilling and reversal, the probability changes in NSWS trends in the random resampling before and after turning points between the observations and CRA-40 were compared. The probability distributions of NSWS trends before and after turning points in CRA-40 were partially similar to those in the observations, while the ranges of changes in NSWS trends in CRA-40 were narrower than those in the observations. According to the results from the random resampling, the annual mean NSWS changes before (after) the turning points in CRA-40 and the observations were  $-0.054 \pm 0.009$  ( $+0.051 \pm 0.032$ ) and  $-0.166 \pm 0.011$  ( $+0.640 \pm 0.159$ )  $\text{m s}^{-1} \text{ decade}^{-1}$ , respectively (Fig. 9c and d).

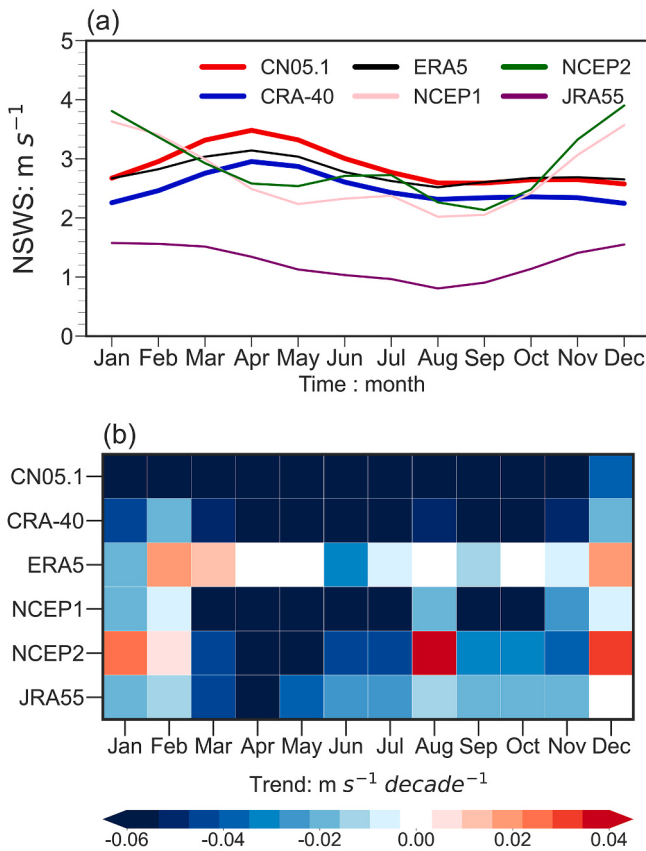


**Fig. 7.** (a) Monthly changes in the averaged NSWS (unit:  $\text{m s}^{-1}$ ), and (b) trends in monthly mean NSWS (unit:  $\text{m s}^{-1} \text{ decade}^{-1}$ ).

#### 4. Discussion

The NSWS changes are sensitive to changes in the surface roughness and topography (Vautard et al., 2010; Guo et al., 2017). Therefore, the scale differences and challenges with topography in models can influence the performance of reanalysis in simulating changes in NSWSs (Fan et al., 2021). In the gridded reanalysis products, each grid-cell value represents the mean wind speed over that area. The gridded spatial variability of NSWS will be small in regions with complex terrain and when the NSWS has a large spatial gradient (Fan et al., 2021). Therefore, with the higher resolution in the reanalyses, more topographical information can be included to better capture the spatial distributions of NSWSs. CRA-40 has a spatial resolution of  $0.312^\circ$  latitude  $\times 0.312^\circ$  longitude, and the spatial resolution of ERA5 can reach  $0.125^\circ$  latitude  $\times 0.125^\circ$  longitude. Therefore, CRA-40 and ERA5 have a higher spatial resolution than the other reanalysis products used in this study, and this aspect could result in the better reproduction of climatological values of NSWS over China by CRA-40 and ERA5 compared to the other reanalyses used in this study.

Compared with other reanalysis products, CRA-40 has the advantage that more observations are assimilated (Liao et al., 2021). Multiple data from conventional observations and satellite instruments, especially over East Asia, have been assimilated into CRA-40 (Wang et al., 2018; Yu et al., 2021). The observations include, but are not limited to, surface station data, radiosondes, aircraft data from the CMA, the Climate Forecast System Reanalysis, the UK Met Office, and the National Maritime Information Center (Li et al., 2021). Although the spatiotemporal resolutions of ERA5 are higher than those of CRA-40, the observed land winds are not assimilated in ERA5 (Hersbach et al., 2020). Therefore, ERA5 could reproduce the climatology of NSWS well over China, but fail to reproduce the stilling. Observational wind data are assimilated in JRA55 (Zhang and Wang, 2020), and therefore, JRA55 also captures the terrestrial stilling over China. Consequently, the assimilation of observations (especially for the observed wind speed) is crucial to improve the performance of reanalysis products in simulating the variations in NSWS. This conclusion also suggests that further improvements are possible with additional observed variables. Additionally, driving forces

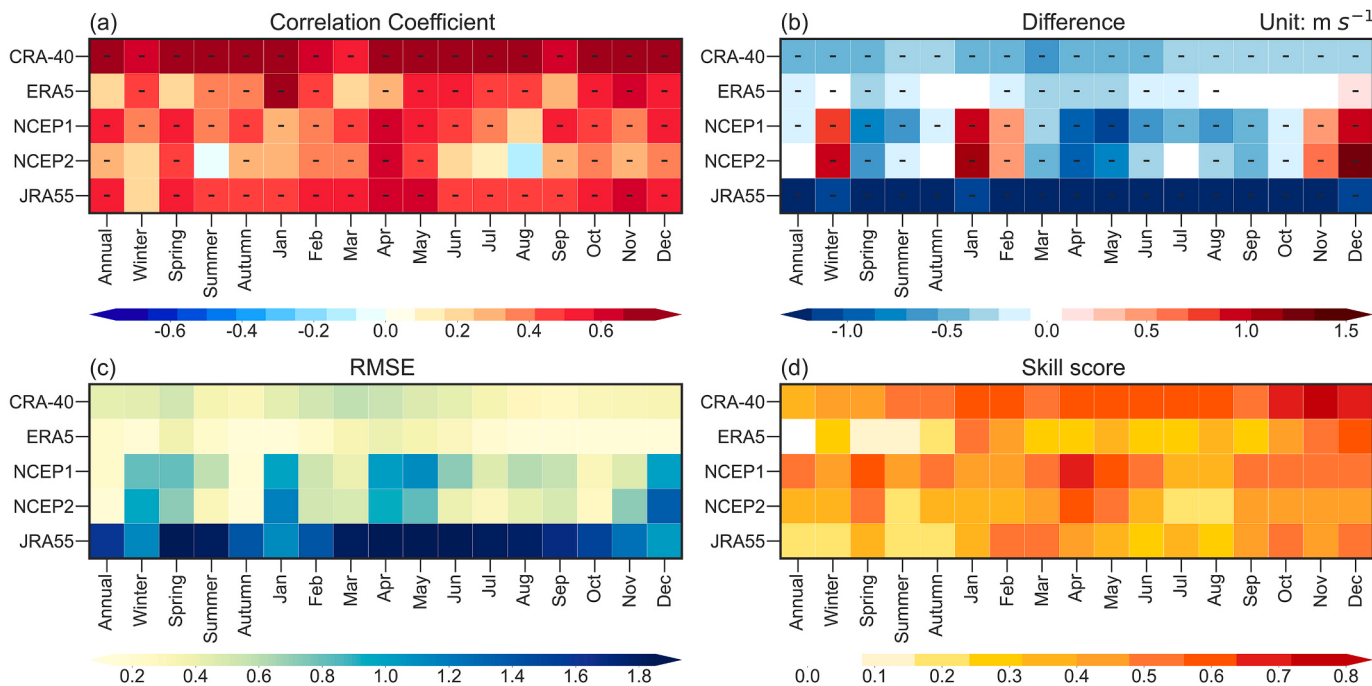


**Fig. 8.** Heat maps of (a) correlation coefficients, (b) NSWS biases (unit:  $\text{m s}^{-1}$ ), (c) root mean square errors (RMSE), and (d) skill scores between observations and reanalysis products. Dashed lines in (a) and (b) denote the correlation coefficients and wind speed differences passing the significance t-test at the 0.10 level.

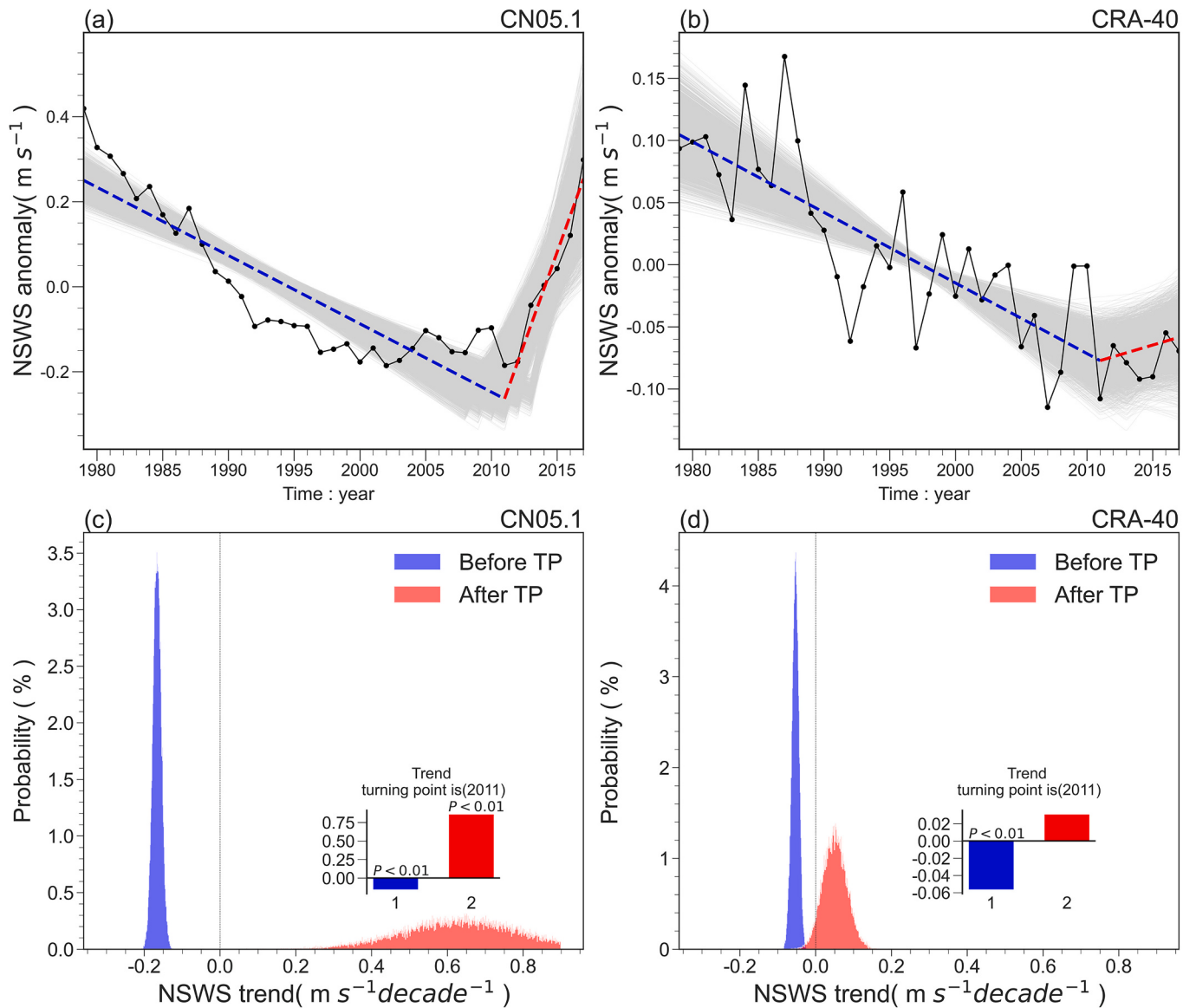


**Fig. 9.** Temporal changes in annual mean NSWS (unit:  $\text{m s}^{-1}$ ) from 1979 to 2017 with (a) CN05.1 observational database and (b) CRA-40, and frequency distributions of the trends in annual mean NSWSS before and after the turning point (TP) identified in the results from 3000 resampling with (c) CN05.1 observational database, and (d) CRA-40. In (a) and (b), each gray line ( $n = 3000$ ) is a piecewise linear fit for a randomly selected 30% subset of all stations. Blue and red lines are piecewise linear fits. The trends during two periods are shown in the inset.  $P < 0.01$  indicate the 99% confidence levels, according to the *t*-test. (For interpretation of the references to colour in this figure legend, the reader is referred to the web version of this article.)

generate the NSWSSs, and changes in large-scale ocean–atmosphere circulations (LOACs) also play a key role on the NSWSS changes (Wu et al., 2018a; Zha et al., 2021c). The changes in LOACs are significantly related to the sea surface temperature. Zeng et al. (2019) found that although atmospheric simulations forced with observed sea surface temperature capture the terrestrial stilling, they fail to reproduce the reversal of stilling. Therefore, a reanalysis that can efficiently simulate the sea surface temperature and LOACs is also capable of better capturing the regional changes in NSWSSs. These aspects will be examined further in a future study.

## 5. Conclusions

The performance of CRA-40 in simulating the spatiotemporal variations in observed NSWSSs was compared with four state-of-the-art global reanalysis products. Potential reasons why CRA-40 best represents the changes in terrestrial NSWSSs over China were discussed. The

major results are listed as follows.

- 1) Compared with NCEP1, NCEP2, and JRA55, CRA-40 and ERA5 better reproduce the spatial distributions of the mean value in NSWSS over China. A significant reduction in NSWSS over China is observed from 1979 to 2017. CRA-40 also shows reductions in NSWSSs, especially in northern, northeastern, and eastern China. However, CRA-40 presents increases in NSWSSs in some parts of western China. ERA5 failed to reproduce the decrease in NSWSS across entire China. The trends in NCEP1 and NCEP2 are not consistent with the observations. JRA55 captures the terrestrial stilling over eastern China; however, the performance of JRA55 was weaker in simulating terrestrial stilling over western China than over eastern China.
- 2) Temporal evolutions of NSWSSs in CRA-40 are closer to those of the observations than those in ERA5, NCEP1, NCEP2, and JRA55. The interannual fluctuations of NSWSSs in CRA-40 are also closer to those of the observations than those of the other reanalysis products.

NCEP1 and NCEP2 overestimate the interannual fluctuations in the observed NSWSSs. The observed NSWSS increases from January to April and then decreases from April to December. CRA-40 and ERA5 produced similar monthly changes in NSWSSs. In contrast, the monthly mean NSWSSs in NCEP1, NCEP2, and JRA55 are not consistent with those of the observations. By comparing the trend of monthly NSWSSs in the observations with that in reanalysis products, we suggest that CRA-40 effectively captures the decreasing trends in monthly NSWSSs. Therefore, the changes in the observed NSWSSs at different time scales are better simulated by CRA-40 than by the other reanalysis products.

The large discrepancies among reanalysis products suggest that users must be cautious when selecting any single dataset for an assessment. Compared with the other reanalysis products, CRA-40 better captures the climatological value, interannual, seasonal, and decadal changes in NSWSSs over China. However, for a specific investigation, the uncertainty of CRA-40 in the assessment must be further quantified to increase confidence in the results. The assimilation of the observed land winds in the reanalysis products is critical in improving the simulation of NSWSSs; therefore, additional observational datasets must be assimilated in the next generation reanalysis product.

#### Data availability statement

The CRA-40 reanalysis products are openly available at <http://www.nmic.cn/analysis/cra40>, last accessed 7 June 2021.

#### Declaration of Competing Interest

The authors declare that they have no known competing financial interests or personal relationships that could have appeared to influence the work reported in this paper.

#### Acknowledgement

The authors cordially thank the anonymous reviewers for their thoughtful comments and constructive suggestions, which significantly improve the quality of this paper. We thank all the data providers. The work is supported by National Key Research and Development Program of China (grant number 2018YFA0606004), National Natural Science Foundation of China (grant numbers 42005023, 41875178, 41775087), Project funded by China Postdoctoral Science Foundation (grant number 2019M660761), and Nanjing Meteorological Bureau Scientific Project (grant number NJ202103). This work is also supported by the Program for Special Research Assistant Project of Chinese Academy of Sciences, the Program for Key Laboratory in University of Yunnan Province, and the Chinese Jiangsu Collaborative Innovation Center for Climate Change, and the C.A.M. was supported by Ramon y Cajal fellowship (RYC-2017-22830) and the grants no. VR-2017-03780 and RTI2018-095749-A-I00 (MCIU/AEI/FEDER, UE).

#### References

- Azorin-Molina, C., et al., 2014. Homogenization and assessment of observed near-surface wind speed trends over Spain and Portugal, 1961–2011. *J. Clim.* 27, 3692–3712.
- Azorin-Molina, C., et al., 2016. Trends of daily peak wind gusts in Spain and Portugal, 1961–2014. *J. Geophys. Res.-Atmos.* 121, 1059–1078.
- Bucchignani, E., Zollo, A.L., Cattaneo, L., Montesarchio, M., Mercogliano, P., 2016. Extreme weather events over China: assessment of COSMO-CLM simulations and future scenarios. *Int. J. Climatol.* 37, 1578–1594.
- Chen, L., Pryor, S.C., Li, D., 2012. Assessing the performance of Intergovernmental Panel on climate Change AR5 climate models in simulating and projecting wind speed over China. *J. Geophys. Res.-Atmos.* 117, D24102.
- Chen, X., Jeong, S., Park, H., Kim, J., Park, C., 2020. Urbanization has stronger impacts than regional climate changes on wind stilling: a lesson from South Korea. *Environ. Res. Lett.* 15, 054016.
- Dadaser-Celik, F., Cengiz, E., 2014. Wind speed trends over Turkey from 1975–2006. *Int. J. Climatol.* 34, 1913–1927.
- Deng, K., Azorin-Molina, C., Minola, L., Zhang, G., Chen, D., 2021. Global near-surface wind speed changes over the last decades revealed by reanalyses and CMIP6 model simulations. *J. Clim.* 34, 2219–2234.
- Fan, W., et al., 2021. Evaluation of Global reanalysis land surface wind speed trends to support wind energy development using in situ observation. *J. Appl. Meteorol. Climatol.* 60, 33–50.
- Fujiwara, M., et al., 2017. Introduction to the SPARC reanalysis Intercomparison project (S-RIP) and overview of the reanalysis systems. *Atmos. Chem. Phys.* 17, 1417–1452.
- Fyllas, N.M., et al., 2009. Basin-wide variations in foliar properties of Amazonian forest: phylogeny, soils and climate. *Biogeosciences* 6, 2677–2708.
- Ge, J., Feng, D., Long, Q., Zhang, W., Zhang, Y., 2021. Characteristics and causes of surface wind speed variations in Northwest China from 1979 to 2019. *Atmos. Res.* <https://doi.org/10.1016/j.atmosres.2021.105527>.
- Guo, H., Xu, M., Hu, Q., 2011. Changes in near-surface wind speed in China: 1969–2005. *Int. J. Climatol.* 31, 349–358.
- Guo, X., Wang, L., Tian, L., Li, X., 2017. Elevation-dependent reductions in wind speed over and around the Tibetan Plateau. *Int. J. Climatol.* 37, 1117–1126.
- He, Y.P., Monahan, A.H., Jones, C.G., Dai, A.G., Biner, S., Caya, D., Winger, K., 2010. Probability distributions of land surface wind speeds over North America. *J. Geophys. Res.-Atmos.* 115, D04103.
- Hersbach, H., et al., 2020. The ERA5 global reanalysis. *Q. J. R. Meteorol. Soc.* 146, 1999–2049.
- Jekel, C., Venter, G., 2019. pwlf: A Python Library for Fitting 1D Continuous Piecewise Linear Functions. [https://github.com/cjekel/piecewise\\_linear\\_fit\\_py](https://github.com/cjekel/piecewise_linear_fit_py).
- Jiang, Y., Luo, Y., Zhao, Z., Tao, S., 2010. Changes in wind speed over China during 1956–2004. *Theor. Appl. Climatol.* 99, 421–430.
- Kalnay, E., et al., 1996. The NCEP/NCAR 40-year reanalysis project. *Bull. Am. Meteorol. Soc.* 77, 437–472.
- Kanamitsu, M., et al., 2002. NCEP–DOE AMIP-II reanalysis (r2). *Bull. Am. Meteorol. Soc.* 83, 1631–1644.
- Kim, J., Paik, K., 2015. Recent recovery of surface wind speed after decadal decrease: a focus on South Korea. *Clim. Dyn.* 45, 1699–1712.
- Kobayashi, S., Ota, Y., Harada, Y., Ebata, A., Moriya, M., Onoda, H., Onogi, K., Kamahori, H., Kobayashi, C., Endo, H., Miyaoka, K., Takahashi, K., 2015. The JRA-55 Reanalysis: General specifications and basic characteristics. *J. Meteorol. Soc. Jpn.* 93, 5–48.
- Laapas, M., Venalainen, A., 2018. Homogenization and trend analysis of monthly mean and maximum wind speed time series in Finland, 1959–2015. *Int. J. Climatol.* 37, 4803–4813.
- Li, Y., Wang, Y., Chu, H., Tang, J., 2008. The climate influence of anthropogenic land-use changes on near-surface wind energy potential in China. *Chin. Sci. Bull.* 53, 2859–2866.
- Li, Y., Chen, Y., Li, Z., Fang, G., 2018. Recent recovery of surface wind speed in Northwest China. *Int. J. Climatol.* 38, 4445–4458.
- Li, C., Zhao, T., Shi, C., Liu, Z., 2020. Evaluation of daily precipitation product in China from the CMA global atmospheric interim reanalysis. *J. Meteorol. Res.* 34, 117–136.
- Li, C., Zhao, T., Shi, C., Liu, Z., 2021. Assessment of precipitation from the CRA40 dataset and new generation reanalysis datasets in the global domain. *Int. J. Climatol.* <https://doi.org/10.1002/joc.7127>.
- Liang, X., Jiang, L., Yan, Y., Shi, C., Zhou, Z., 2020. A 10-yr global land surface reanalysis interim dataset (CRA-Interim/Land): Implementation and preliminary evaluation. *J. Meteorol. Res.* 34, 101–116.
- Liao, J., Wang, H., Zhou, Z., Liu, Z., Jiang, L., Yuan, F., 2021. Integration, quality assurance, and usage of global aircraft observations in CRA. *J. Meteorol. Res.* 35, 1–16.
- Liu, X., Zhang, X.J., Tang, Q., Zhang, X.Z., 2014. Effects of surface wind speed decline on modeled hydrological conditions in China. *Hydrol. Earth Syst. Sci.* 18, 2803–2813.
- Malloy, J.W., et al., 2015. A surface wind extremes (“wind Lulls” and “Wind Blows”) Climatology for Central North America and Adjoining Oceans (1979–2012). *J. Appl. Meteorol. Climatol.* 54, 643–657.
- McVicar, T.R., Van Niel, T.G., Li, L.T., Roderick, M.L., Rayner, D.P., Ricciardulli, L., Donohue, R., 2008. Wind speed climatology and trends for Australia, 1975–2006: Capturing the stilling phenomenon and comparison with near-surface reanalysis output. *Geophys. Res. Lett.* 35, L20403.
- McVicar, T.R., et al., 2012. Global review and synthesis of trends in observed terrestrial near-surface wind speeds: implications for evaporation. *J. Hydrol.* 24, 182–2015.
- Peng, D., Zhou, T., Zhang, L., Zhang, W., Chen, X., 2020. Observationally constrained projection of the reduced intensification of extreme climate events in Central Asia from 0.5 °C less global warming. *Clim. Dyn.* 54, 543–560.
- Pryor, S.C., Ledolter, J., 2010. Addendum to “Wind speed trends over the contiguous United States”. *J. Geophys. Res.-Atmos.* 115, 1159–1171.
- Pryor, S.C., et al., 2009. Wind speed trends over the contiguous United States. *J. Geophys. Res.-Atmos.* 114, 1159–1171.
- Pryor, S.C., Barthelmie, R.J., Bukovsky, M.S., Leung, R., Sakaguchi, K., 2020. Climate change impacts on wind power generation. *Nat. Rev. Earth Environ.* 1, 627–643.
- Ramon, J., Lledo, L., Torralba, V., Soret, A., Doblas-Reyes, F.J., 2019. What global reanalysis best represents near-surface winds? *Q. J. R. Meteorol. Soc.* 145, 3236–3251.
- Roderick, M.L., Rotstayn, L.D., Farquhar, G.D., Hobbins, M.T., 2007. On the attribution of changing pan evaporation. *Geophys. Res. Lett.* 34, 251–270.
- Shen, C., Zha, J., Wu, J., Zhao, D., 2021a. Centennial-scale variability of terrestrial near-surface wind speed over China from reanalysis. *J. Clim.* 34, 5829–5846.
- Shen, C., Zha, J., Zhao, D., Wu, J., Fan, W., Yang, M., Li, Z., 2021b. Estimating centennial-scale changes in global terrestrial near-surface wind speed based on CMIP6 GCMs. *Environ. Res. Lett.* 16, 084039.

- Sherman, P., Song, S., Chen, X., Chen, M., 2021. Projected changes in wind power potential over China and India in high resolution climate models. *Environ. Res. Lett.* 16, 034057.
- Song, P., Zhou, T., 2014. The climatology and interannual variability of East Asian summer monsoon in CMIP5 coupled models: does air-sea coupling improve the simulations. *J. Clim.* 27, 8761–8777.
- Storn, R., Price, K., 1997. Differential Evolution-a simple and efficient heuristic for global optimization over continuous spaces. *J. Glob. Optim.* 11, 341–359.
- Sun, B., Wang, H.J., 2014. Inter-decadal transition of the leading mode of inter-annual variability of summer rainfall in East China and its associated atmospheric water vapor transport. *Clim. Dyn.* 44, 2703–2722.
- Tian, Q., Huang, G., Hu, K., Niyogi, D., 2019. Observed and global climate model based changes in wind power potential over the Northern Hemisphere during 1979–2016. *Energy* 167, 1224–1235.
- Vautard, R., Cattiaux, J.L., Yiou, P., Thepaut, J.N., Ciais, P., 2010. Northern Hemisphere atmospheric stilling partly attributed to an increase in surface roughness. *Nat. Geosci.* 3, 756–761.
- Wan, H., Wang, X.L., Swail, V.R., 2010. Homogenization and trend analysis of Canadian near-surface wind speeds. *J. Clim.* 23, 1209–1225.
- Wang, R., et al., 2017. Variation of strong dust storm events in Northern China during 1978–2007. *Atmos. Res.* 183, 166–172.
- Wang, M., Yao, S., Jiang, L., Liu, Z., Shi, C., Hu, K., Zhang, T., Zhang, Z., Liu, J., 2018. Collection and preprocessing of satellite remote-sensing data in CRA-40 (CMA's global atmospheric reanalysis). *Adv. Meteorol. Sci. Technol.* 8, 158–163.
- Wang, J., Feng, J., Yan, Z., Zha, J., 2020. Urbanization impact on regional wind stilling: a modeling study in the Beijing-Tianjin-Hebei region of China. *J. Geophys. Res.-Atmos.* 125 (e2020JD033132).
- Wu, J., Gao, X., 2013. A gridded daily observation dataset over China region and comparison with the other datasets. *Chin. J. Geophys.* 56, 1102–1111.
- Wu, J., Gao, X., Gao, F., Chen, Z., Chen, D., 2012. Climate effects of the three Gorges Reservoir as simulated by a high resolution double nested regional climate model. *Quat. Int.* 282, 27–36.
- Wu, J., Zha, J., Zhao, D., 2016. Estimating the impact of the changes in land use and cover on the surface wind speed over the East China plain during the period 1980–2011. *Clim. Dyn.* 46, 847–863.
- Wu, J., Zha, J., Zhao, D., 2017. Evaluating the effects of land use and cover change on the decrease of surface wind speed over China in recent 30 years using a statistical downscaling method. *Clim. Dyn.* 48, 131–149.
- Wu, J., Zha, J., Zhao, D., Yang, Q., 2018a. Changes in terrestrial near-surface wind speed and their possible causes: an overview. *Clim. Dyn.* 51, 2039–2078.
- Wu, J., Zha, J., Zhao, D., Yang, Q., 2018b. Effects of surface friction and turbulent mixing on long-term changes in the near-surface wind speed over the eastern China plain from 1981 to 2010. *Clim. Dyn.* 51, 2285–2299.
- Wu, J., Zha, J., Zhao, D., Yang, Q., 2018c. Changes of wind speed at different heights over eastern China during 1980–2011. *Int. J. Climatol.* 38, 4476–4495.
- Xu, M., Chang, C.P., Fu, C., Qi, Y., Robock, A., Robinson, D., Zhang, H., 2006. Steady decline of East Asian monsoon winds, 1969–2000: evidence from direct ground measurements of wind speed. *J. Geophys. Res.-Atmos.* 111, D24111.
- You, Q., et al., 2010. Decreasing wind speed and weakening latitudinal surface pressure gradients in the Tibetan Plateau. *Clim. Res.* 42, 57–64.
- You, Q., et al., 2014. Observed surface wind speed in the Tibetan Plateau since 1980 and its physical causes. *Int. J. Climatol.* 34, 1873–1882.
- Yu, X., Zhang, L., Zhou, T., Liu, J., 2021. The Asian Subtropical Westerly Jet Stream in CRA-40, ERA5, and CFSR reanalysis data: comparative assessment. *J. Meteorol. Res.* 35, 46–63.
- Zeng, Z., et al., 2019. A reversal in global terrestrial stilling and its implications for wind energy production. *Nat. Clim. Chang.* 9, 979–985.
- Zha, J., Wu, J., Zhao, D., 2016. Changes of probabilities in different wind grades induced by land use and cover change in eastern China plain during 1980–2011. *Atmos. Sci. Lett.* 17, 264–269.
- Zha, J., Wu, J., Zhao, D., 2017a. Effects of land use and cover change on the near-surface wind speed over China in the last 30 years. *Prog. Phys. Geogr. Earth Environ.* 41, 46–67.
- Zha, J., Wu, J., Zhao, D., Yang, Q., 2017b. Changes of the probabilities in different ranges of near-surface wind speed in China during the period for 1970–2011. *J. Wind Eng. Ind. Aerodyn.* 169, 156–167.
- Zha, J., Wu, J., Zhao, D., Tang, J., 2019a. A possible recovery of the near-surface wind speed in eastern China during winter after 2000 and the potential causes. *Theor. Appl. Climatol.* 136, 119–134.
- Zha, J., Zhao, D., Wu, J., Zhang, P., 2019b. Numerical simulation of the effects of land use and cover change on the near-surface wind speed over eastern China. *Clim. Dyn.* 53, 1783–1803.
- Zha, J., Shen, C., Zhao, D., Wu, J., Fan, W., 2021a. Slowdown and reversal of terrestrial near-surface wind speed and its future changes over eastern China. *Environ. Res. Lett.* 16, 034028.
- Zha, J., Zhao, D., Wu, J., Shen, C., 2021b. Research progress and prospects of terrestrial near-surface wind speed variations in China. *J. Meteorol. Res.* 35, 1–21.
- Zha, J., Shen, C., Li, Z., Wu, J., Zhao, D., Fan, W., Sun, M., Azorin-Molina, C., Deng, K., 2021c. Projected changes in global terrestrial near-surface wind speed in 1.5 °C-4.0 °C global warming levels. *Environ. Res. Lett.* 16, 114016.
- Zhang, Z., Wang, K., 2020. Stilling and recovery of the surface wind speed based on observation, reanalysis, and geostrophic wind theory over China from 1960 to 2017. *J. Clim.* 30, 3989–4008.
- Zhang, Z., Wang, K., Chen, D., Li, J., Dickinson, R., 2019. Increase in surface friction dominates the observed surface wind speed decline during 1973–2014 in the northern Hemisphere lands. *J. Clim.* 32, 7421–7435.
- Zhang, Y., Gao, L., Cao, L., Yan, Z., Wu, Y., 2020. Decreasing atmospheric visibility associated with weakening winds from 1980–2017 over China. *Atmos. Environ.* 224, 117314.
- Zhang, G., Azorin-Molina, C., Chen, D., McVicar, T.R., Guijarro, J.A., Kong, F., Minola, L., Deng, K., Shi, P., 2021. Uneven warming likely contributed to declining near-surface wind speeds in northern China between 1961 and 2016. *J. Geophys. Res.-Atmos.* <https://doi.org/10.1029/2020JD033637>.
- Zhao, D., Zhang, L., Zhou, T., Liu, J., 2021. Contributions of local and remote atmospheric moisture fluxes to East China precipitation estimated from CRA-40 reanalysis. *J. Meteorol. Res.* 35, 32–45.